Arch. Metall. Mater. **64** (2019), 2, 525-530

DOI: 10.24425/amm.2019.127571

DONG-YEOL WI*, YOUNG-KYUN KIM*, TAE-SIK YOON**, KEE-AHN LEE*#

MICROSTRUCTURE AND HIGH TEMPERATURE OXIDATION PROPERTIES OF Fe-Cr-Ni HK30 ALLOY MANUFACTURED BY METAL INJECTION MOLDING

This study investigated the microstructure and high temperature oxidation properties of Fe-25Cr-20Ni-1.5Nb, HK30 alloy manufactured by metal injection molding (MIM) process. The powder used in MIM had a bi-modal size distribution of 0.11 and 9.19 μm and had a spherical shape. The initial powder consisted of γ-Fe and $Cr_{23}C_6$ phases. Microstructural observation of the manufactured (MIMed) HK30 alloy confirmed $Cr_{23}C_6$ along the grain boundary of the γ-Fe matrix, and NbC was distributed evenly on the grain boundary and in the grain. After a 24-hour high temperature oxidation test at air atmospheres of 1000, 1100 and 1200°C, the oxidation weight measured 0.72, 1.11 and 2.29 mg/cm,^{2} respectively. Cross-sectional observation of the oxidation specimen identified a dense Cr_2O_3 oxide layer at 1000°C condition, and the thickness of the oxide layer increased as the oxidation temperature increased. At 1100°C and 1200°C oxidation temperatures, Fe-rich oxide was also formed on the dense Cr_2O_3 oxide layer. Based on the above findings, this study identified the high-temperature oxidation mechanism of HK30 alloy manufactured by MIM.

Keywords: Metal injection molding, HK30, Microstructure, High temperature oxidation

1. Introduction

HK30 alloy is modified by adding Nb to A310 austenite stainless steel, and it has greater high temperature strength and creep properties compared to conventional A310 steel [1,2]. HK30 alloy has a microstructure that contains high temperature stable phase NbC in the grain boundary along with the austenite matrix [3]. In general, HK30 alloy is manufactured using casting, and it is commonly used for complex shaped high-temperature parts such as turbochargers and heat exchangers. However, parts made using casting are vulnerable to property degradation due to interior defects. Due to this, a process capable of producing complex shapes using a net shape without defects is being demanded, and one of the processes anticipated to replace conventional processes is metal injection molding (MIM).

MIM is a process that uses a feedstock mixing metal powder and polymer binder, builds the shape using injection molding, removes the binder by debinding and applying sintering to finalize the net shape component [4]. The final product manufactured using MIM can accurately estimate the product's dimensions, so the process is very economical. The surface condition of the final product manufactured using MIM is outstanding. Also, as MIM can produce products with complex shapes nearing theoretical density with a suitable mix of a binder and metal powder, the process is acceptable for producing parts when excellent performance is demanded.

Generally, HK30 alloy manufactured by MIM can be used as high temperature structural material. High temperature oxidation properties are important for the HK30 alloy to be used as a high temperature structural material. Although the mechanical properties of MIMed HK30 alloy have been presented so far, study on the high temperature oxidation property is still insufficient.

Therefore, this study manufactured HK30 alloy using MIM and investigated its microstructure and high temperature oxidation properties. In addition, this study examined the microstructural evolution and oxide phases of HK30 alloy to identify the high temperature oxidation mechanism.

2. Experimental

Fig. 1(a) and (b) show the microstructure and phase analysis results of the powder used in this study, and Fig. 1(c) is the particle size distribution of HK30 powder. The HK30 alloy powder used a bi-modal feedstock with an average particle size of approximately 0.11 and 9.19 μm. Most of the powder had a spherical shape, and phase analysis confirmed that the powder consisted of γ-Fe and $Cr_{23}C_6$ phases.

The above powder is mixed with a suitable binder based on the know-how of Bestner Co., and injection molding was performed. To remove the binder after injection molding, debinding

* INHA UNIVERSITY, DEPARTMENT OF MATERIALS SCIENCE & ENGINEERING, INCHEON 22212, REPUBLIC OF KOREA
** BESTNER CO., EUMSEONG, CHUNGCHEOGBUK-DO 27623, REPUBLIC OF KOREA
# Corresponding author: keeahn@inha.ac.kr

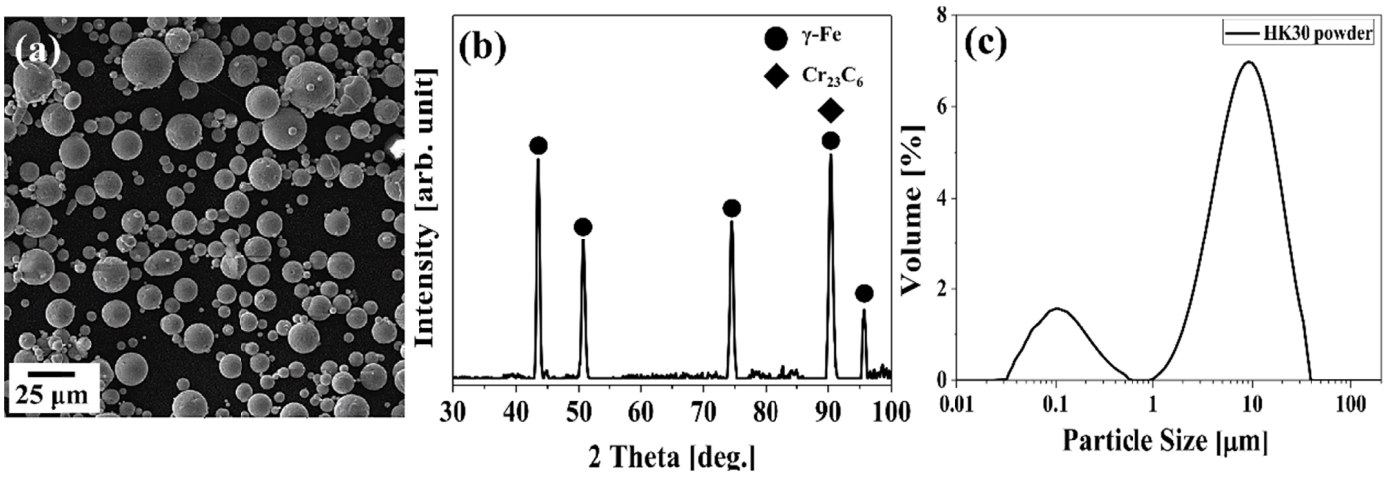

Fig. 1. HK30 powder feedstock analysis results: (a) powder shape, (b) XRD analysis, and (c) particle size distribution

was performed at 40°C, heptan atmosphere for 12 hours, and then sintering was performed at 1,285°C, argon atmosphere for 2 hours.

The MIMed HK30 alloy was polished with SiC paper (#100~#2000) and then mirror polished using diamond suspension (1 μm) to observe its microstructure. Microstructure and phase analysis were performed using a scanning electron microscope (SEM, VEGA II LMU), X-ray diffraction (XRD, Ultima IV) and electron probe micro analysis (EPMA, EPMA-1600) equipment. The high temperature oxidation test of the MIMed HK30 alloy was performed in a box furnace at 1000, 1100 and 1200°C in air atmosphere for 24 hours. The heating rate was 10°C/min. The oxidized specimen was furnace cooled after oxidation test. The weight before and after oxidation were measured to calculate the weight gain.

3. Results and discussion

Fig. 2 shows the microstructure and phase analysis results of the MIMed HK30 alloy. Initial microstructural observation of the MIMed HK30 alloy (Fig. 2(a)) measured an average grain size of approximately 22.12 μm. In addition, the manufactured material had a high density with a porosity of 0.087%. The high density obtained in the MIMed HK30 alloy can be suspected to be due to the liquid phase sintering effect of a suitable condition. Fig. 2(b) is the XRD phase analysis results of the MIMed HK30 alloy, and it shows γ-Fe and $Cr_{23}C_6$ phases just like the initial powder phases. Fig. 2(a) shows that the Cr-based carbides are mainly found in the grain boundary, and Nb-based carbides are evenly distributed in the grain and on the grain boundary. Table 1 shows the chemical compositions of MIMed HK30 alloy analyzed by using XRF (X-ray fluorescence). The composition of MIMed material was well accord with the standard composition of HK30 alloy.

The high temperature oxidation properties of MIMed HK30 alloy are shown in Fig. 3. Oxidation weight gain in an air atmosphere at 1000, 1100 and 1200°C conditions for 24 hours measured 0.72, 1.11 and 2.29 mg/cm^{2,} respectively. The weight gain of conventional Fe-25Cr-20Ni alloy manufactured by casting with identical oxidation conditions at 1000°C is reported to be 1.1 mg/cm^2 [6]. By comparison, the 1000°C oxidation property of the MIMed Fe-Cr-Ni of this study achieved greater high temperature oxidation resistance compared to conventional Fe-25Cr-20Ni alloy. The greater high temperature oxidation resistance of the MIMed HK30 alloy is suspected to be due to the high density of material and formation of NbC. In other words, the affinity of Nb, which is distributed evenly in the grain and on the grain boundary, with C is higher than the affinity of Cr with C and is suspected to have resulted in the restriction of Cr carbide formation and the prevention of internal grain boundary oxidation.

Fig. 4 shows the MIMed HK30 alloy phase analysis results after a high temperature oxidation test. γ-Fe and Cr_2O_3 phases were found in all oxidation conditions (1000, 1100, 1200°C). In the case of 1100°C, Fe-rich oxides began to form, and in the case of 1200°C, Ni-based oxides were also found.

Fig. 5 is the cross-sectional observation result of HK30 alloy oxidation specimen with each temperature condition. At 1000°C, the cross-sectional observation confirmed that a dense Cr oxide of approximately 5.4 μm was formed. It is well-known that high Cr containing steel forms dense Cr_2O_3. This dense

TABLE 1

Chemical composition of MIMed HK30 alloy (wt.%)

	Fe	Cr	Ni	Si	Mn	C	Nb
MIM	Bal.	24.33	21.21	1.20	1.55	—	1.44
Standard	Bal.	24~27	19~22	0.75~1.30	1.5	0.25~0.50	1.2~1.5

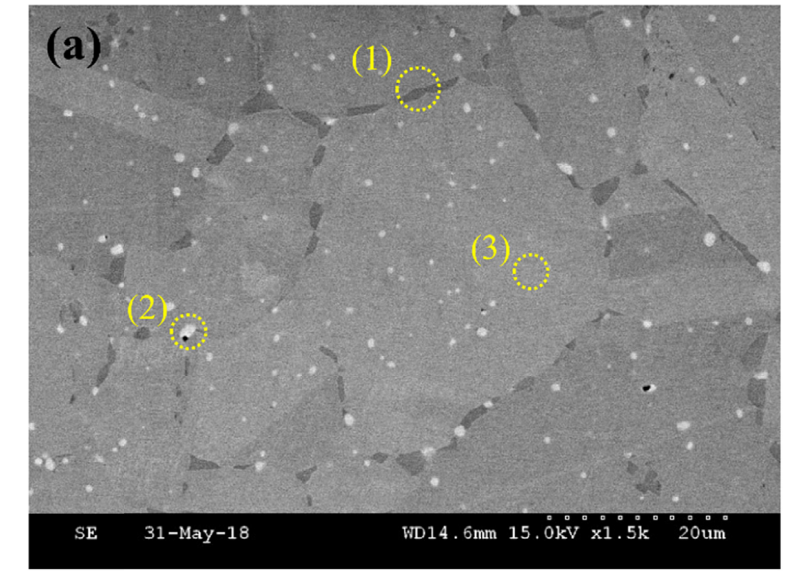

(1)

Elt.	Conc.	Units
C	7.48	wt.%
Cr	69.18	wt.%
Fe	18.70	wt.%
Ni	4.64	wt.%
	100.00	wt.%

(2)

Elt.	Conc.	Units
C	7.47	wt.%
Cr	4.90	wt.%
Fe	7.40	wt.%
Ni	2.47	wt.%
Nb	77.76	wt.%
	100.00	wt.%

(3)

Elt.	Conc.	Units
Si	1.15	wt.%
Cr	24.18	wt.%
Fe	52.71	wt.%
Ni	21.96	wt.%
	100.00	wt.%

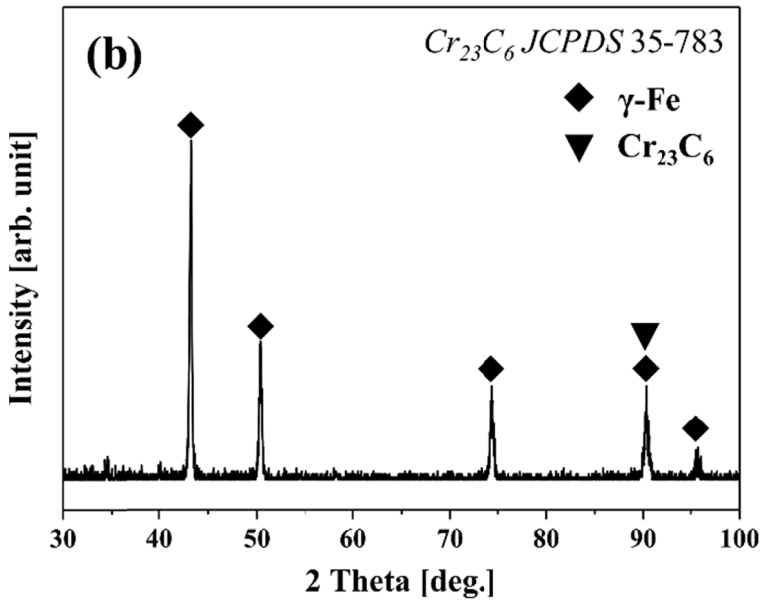

Fig. 2. (a) Microstructure, EDS analysis and (b) XRD phase analysis results of MIMed HK30 alloy

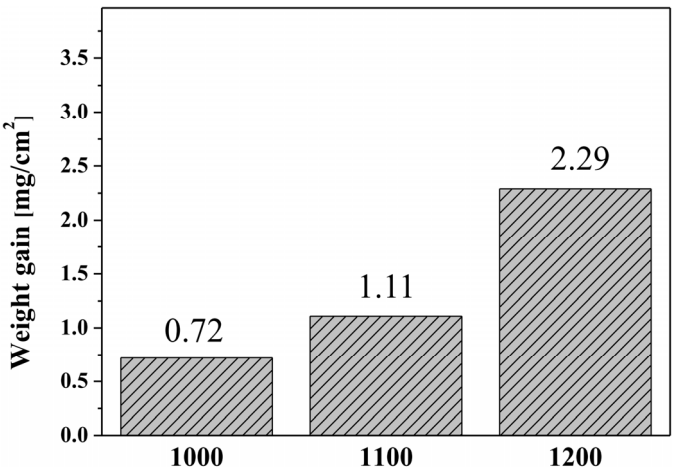

Fig. 3. Weight gains of the oxidized samples at 1000, 1100, and 1200°C (24 hrs)

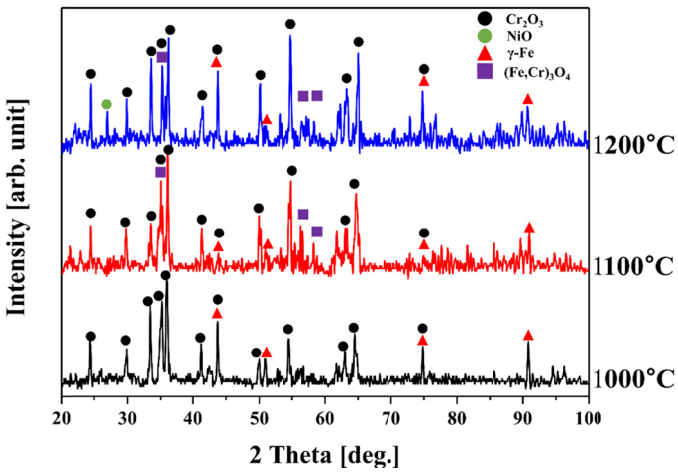

Fig. 4. XRD phase analysis results after high temperature oxidation tests of MIMed HK30 alloy

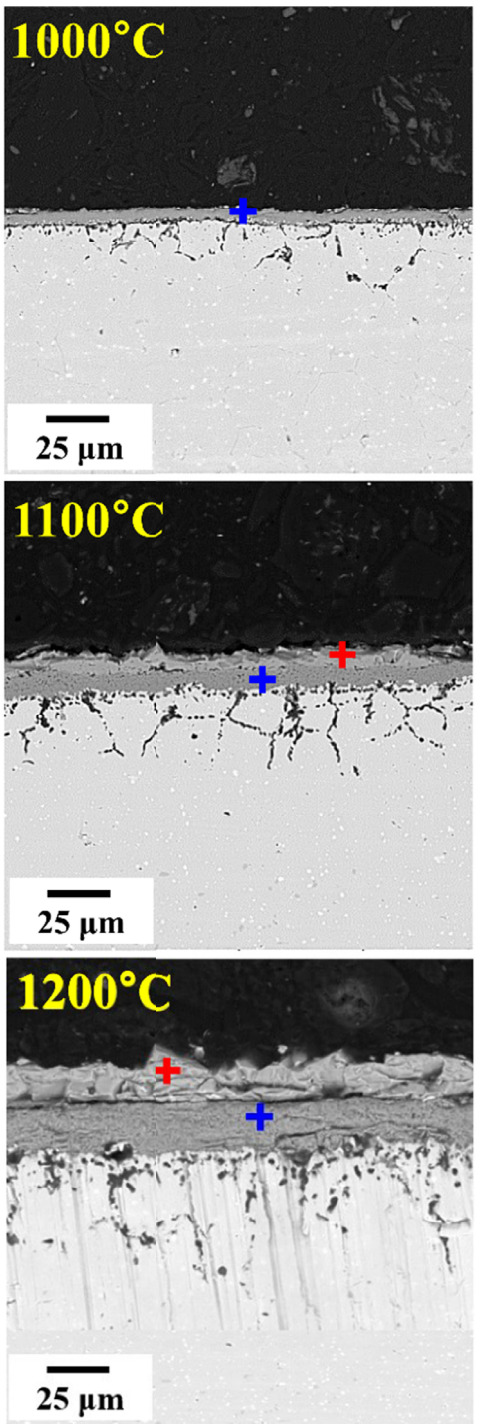

Elt.	Conc	Units
C	2.498	wt.%
O	32.579	wt.%
Cr	54.282	wt.%
Fe	7.405	wt.%
Ni	2.580	wt.%
Nb	0.655	wt.%
	100.000	wt.%

Elt.	Conc	Units
C	5.536	wt.%
O	35.496	wt.%
Cr	16.317	wt.%
Fe	30.833	wt.%
Ni	11.647	wt.%
Nb	0.170	wt.%
	100.000	wt.%

Elt.	Conc	Units
C	0.887	wt.%
O	32.682	wt.%
Cr	63.113	wt.%
Fe	1.570	wt.%
Ni	0.267	wt.%
Nb	1.481	wt.%
	100.000	wt.%

Elt.	Conc	Units
C	5.536	wt.%
O	35.496	wt.%
Cr	16.317	wt.%
Fe	30.833	wt.%
Ni	11.647	wt.%
Nb	0.170	wt.%
	100.000	wt.%

Elt.	Conc	Units
C	0.887	wt.%
O	32.682	wt.%
Cr	63.113	wt.%
Fe	1.570	wt.%
Ni	0.267	wt.%
Nb	1.481	wt.%
	100.000	wt.%

Fig. 5. Cross-sectional SEM observation results of MIMed HK30 alloy after oxidation at 1000, 1100, and 1200°C

Cr_2O_3 oxide layer is reported to improve oxidation properties by preventing the dispersion of ions and electrons such as Fe [7,8]. Meanwhile, internal grain boundary oxidation was observed near the substrate surface. It was found in the initial microstructure of MIMed HK30 alloy (Fig. 2) that Cr-based carbides segregate at the grain boundary. It can induce Cr depletion around the grain boundary and result in the internal grain boundary oxidation (Fig. 5). Cross-sectional observation of the 1100°C specimen confirmed that the thickness of Cr_2O_3 oxide film increased by approximately 6.75 μm, and Fe-rich based oxide layer of approximately 5.13 μm was also found on the Cr_2O_3 oxide layer. The total thickness of oxides found in the 1100°C specimen was 11.88 μm. In the case of the 1100°C oxidation condition, the internal grain boundary oxidation infiltrated deeper than the 1000°C condition. The 1200°C oxidation condition specimen had a dense Cr_2O_3 oxide layer of approximately 20.1 μm thick, and the thickness of Fe-rich based oxide layer increased to 16.2 μm. The total oxide thickness measured 36.3 μm (1200°C), which was a significant increase over the 1100°C temperature condition. In addition, the internal grain boundary oxidation deepened as the oxidation temperature increased, and the circular void became to be more significant.

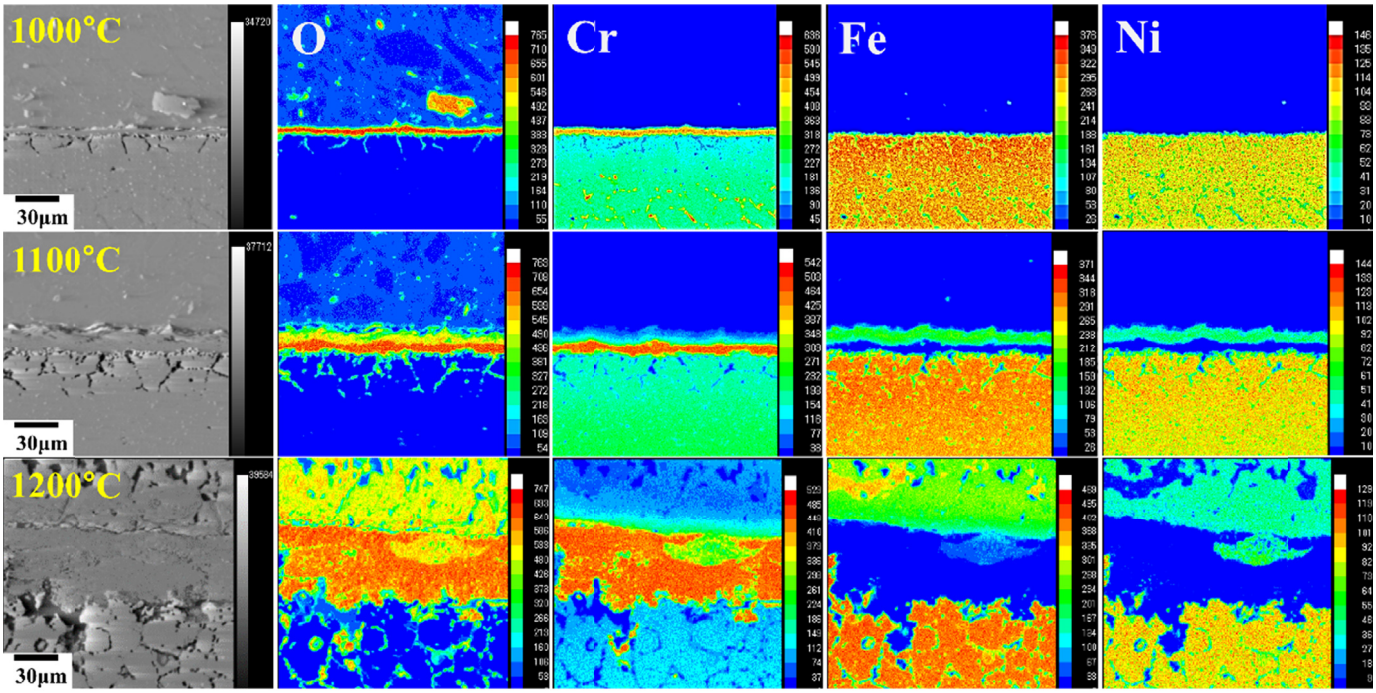

Fig. 6. EPMA analysis results of the cross-section of HK30 alloy after oxidation at 1000,1100, and 1200°C

The EPMA analysis results of HK30 oxidation specimen are shown in Fig. 6. As shown in the cross-sectional observation of the 1000°C oxidation specimen, a dense Cr_2O_3 oxide film with approximately 5 μm thickness was formed on the surface. The Cr content in the oxidation specimen surface had lower intensity than the specimen interior, and the Cr content in the grain boundary also had low intensity. The Cr depletion on the HK30 alloy surface and grain boundary are due to the $Cr_{23}C_6$ phase present in the initial specimen's grain boundary and the diffusion of Cr ions present on the specimen surface. As the oxidation temperature increases to 1100 and 1200°C, the Cr depletion at the specimen surface and the internal oxidation through the internal grain boundary deepens. Furthermore, the additional Fe-rich oxides formed on the Cr_2O_3 oxide are confirmed once again. This can be suspected to be the result of the oxidation behavior of the positive carrier type material. In other words, Cr_2O_3 is a p-type oxide that forms a void due to insufficient metal ions at the interstitial site in the oxide. This void has a greater concentration in air/oxide interface than in metal/oxide interface. In other words, according to the void concentration at the two interfaces, the metal ions inside the specimen move to occupy the voids present in the air/oxide, forming a (Fe, Cr, Ni)-based oxide on the Cr_2O_3 oxide.

As a result, MIMed HK30 alloy forms thicker surface oxides and deeper internal oxidation as oxidation temperature increases from 1000°C to 1100 and 1200°C. However, maintaining a dense condition without spallation and internal pores in the oxidation layer at high temperatures such as 1000~1200°C is an indication of outstanding oxidation resistance property. As such, the superior oxidation resistance property of the MIMed HK30 alloy can be explained by the high density characteristic with almost no defect and the NbC phase present inside the alloy.

4. Conclusions

This study manufactured an Fe-25Cr-20Ni-1.5Nb alloy, HK30, using MIM, and investigated its microstructure and high temperature oxidation properties. The initial microstructural observation confirmed $Cr_{23}C_6$ phase along the grain boundary of the γ-Fe matrix, and the high temperature stable phase, NbC, was evenly formed in the grain and grain boundary.

High temperature oxidation tests at 1000, 1100 and 1200°C measured weight gain of 0.72, 1.11 and 2.29 mg/cm^2, respectively. Dense oxide layer, Cr_2O_3, was formed in all oxidation temperatures, and internal oxidation occurred along the grain boundary. At 1100°C oxidation temperature, Fe-rich based oxides were formed on Cr-based oxides, and an additional Ni-based oxides were found at the 1200°C condition. The outstanding high temperature oxidation resistance of MIMed HK30 material is achieved due to the NbC phase present in the grain and grain boundary.

EPMA analysis of the high temperature oxidation specimen confirmed that (Fe, Cr, Ni)-based oxides were formed on the dense Cr_2O_3 oxide at temperatures of 1100°C and above. The formation and development of (Fe, Cr, Ni) based oxides on Cr_2O_3 oxide are identified to be due to the metal ions moving caused by the concentration gradient of numerous voids present in the air/oxide interface based on the oxidation mechanism of positive carrier type materials.

Acknowledgments

This work was supported by INHA University Research Grant (INHA-57819-01)

REFERENCES

[1] T. Sourmail, Mater. Sci. Technol. **17**, 1 (2001).
[2] H.R.H. Bajguirani, Mater. Sci. Eng. A **338**, 142 (2002).
[3] M. Ekstrom, S. Jonsson, Mater. Sci. Eng. A **616**, 78 (2014).
[4] C.H. Ji, N.H. Loh, K.A. Khor, S.B. Tor, Mater. Sci. Eng. A **311**, 74 (2001).
[5] Y.-K. Kim, T.-S. Yoon, K.-A. Lee, Korean J. Met. Mater. **56**, 121 (2018).
[6] J.E. Croll, G.R. Wallwork, Oxid. Met. **4**, 121 (1972).
[7] R. Bauer, M. Baccalaro, L.P.H. Jeurgens, M. Pohl, E.J. Mittemeijer, Oxid. Met. **69**, 265 (2008).
[8] N. Madem, J. Monnier, R.B. Hadjean, A. Steckmeyer, J.M. Joubert, Corrosion Sci. **132**, 223 (2018).